2019

Methods for Monitoring Matrix-Induced Autophagy.

Carolyn Chen
Thomas Jefferson University, carolyn.chen@jefferson.edu

Aastha Kapoor
Thomas Jefferson University, aastha.kapoor@jefferson.edu

Renato V. Iozzo
Thomas Jefferson University, renato.iozzo@jefferson.edu

Methods for Monitoring Matrix-Induced Autophagy

Carolyn Chen*, Aastha Kapoor* and Renato V. Iozzo

Department of Pathology, Anatomy and Cell Biology and the Cancer Cell Biology and Signaling Program, Sidney Kimmel Medical College at Thomas Jefferson University, Philadelphia, PA 19107, USA

*Contributed equally to this work

Email of Corresponding Author: renato.iozzo@jefferson.edu

Methods for Monitoring Matrix-Induced Autophagy

Carolyn Chen*, Aastha Kapoor* and Renato V. Iozzo

Department of Pathology, Anatomy and Cell Biology and the Cancer Cell Biology and Signaling Program, Sidney Kimmel Medical College at Thomas Jefferson University, Philadelphia, PA 19107, USA

Running Head: Monitoring Matrix-Induced Autophagy

Summary

A growing body of research demonstrates modulation of autophagy by a variety of matrix constituents, including decorin, endorepellin, and endostatin. These matrix proteins are both pro-autophagic and anti-angiogenic. Here, we detail a series of methods to monitor matrix-induced autophagy and its concurrent effects on angiogenesis. We first discuss cloning and purifying proteoglycan fragment and core proteins in the laboratory and review relevant techniques spanning from cell culture to treatment with these purified proteoglycans *in vitro* and *ex vivo*. Further, we cover protocols in monitoring autophagic progression via morphological and microscopic characterization, biochemical western blot analysis, and signaling pathway investigation. Downstream angiogenic effects using *in vivo* approaches are then discussed using wild-type mice and the GFP-LC3 transgenic mouse model. Finally, we explore matrix-induced mitophagy via monitoring changes in mitochondrial DNA and permeability.

Key words: Decorin; endorepellin; LC3; Beclin 1; mitophagy; LC3-GFP; starvation; angiogenesis

1. Introduction

A vast and complex reservoir, the extracellular matrix (ECM) contributes an abundance of dynamic roles to surrounding cells to maintain tissue homeostasis and sustain development ***(1-16)***. A major constituent of the ECM, proteoglycans fulfill a range of structural and signaling roles that regulate cellular processes including endocytosis ***(17-20),*** cell adhesion ***(21-24)***, inflammation and wound healing **(25,26)**, thrombosis ***(27)***, angiogenesis ***(28-31)***, and autophagy ***(32-34)***. Autophagy is the "self-eating" process by which cells deliver intracellular proteins, lipids and organelles to lysosomal compartments for degradation and recycling. Independent of nutrient deprivation, several matrix constituents effectively modulate this intracellular degradative pathway, among which are decorin, endorepellin, endostatin, and kringle V ***(35)***.

Decorin, a small leucine-rich proteoglycan (SLRP), functions as a pan-receptor tyrosine kinase inhibitor and impedes endothelial cell migration while activating autophagy ***(32,36,37)***. Similarly, endostatin, ~~is~~ the 20-kDa C terminal fragment of collagen XVIII-α1, exerts its angiostatic activity by binding to $\alpha5\beta1$ integrin and inducing autophagy through Vps34, Beclin 1, and LC3-II ***(38,39)***. Kringle V, instead, is an internal proteolytic fragment of plasminogen that induces autophagy in endothelial cells via binding to glucose-regulated protein 78 kDa (GRP78) while exhibiting potent anti-angiogenic effects on endothelial cell migration and proliferation ***(40)***.

Endorepellin is the proteolytically processed C terminal fragment of the substantial heparan sulfate proteoglycan perlecan ***(41,42)*** a proteoglycan with a complex biology ***(43-48)***involved in the regulation of angiogenesis, both developmental and experimental ***(28,49-52).*** Located in the basement membrane of vascular endothelial cells, endorepellin has recently emerged as a soluble pro-autophagic and anti- angiogenic molecule of the ECM, inhibiting endothelial cell migration, capillary morphogenesis, and proliferation ***(53-59)***. Through its three laminin-like globular (LG) domains and partial agonistic activity, it signals dually through vascular endothelial growth factor receptor 2 (VEGFR2) to induce protracted autophagy and the α2β1 integrin for actin cytoskeleton dissolution, leading to an anti-migratory and angiostatic phenotype ***(55,60-63)***. Downstream of endorepellin signaling through VEGFR2, 5'–adenosine monophosphate-activated protein kinase (AMPK) is

phosphorylated at Thr172, leading to inhibition of mammalian target of rapamycin (mTOR) and induction of autophagy markers including paternally-expressed gene 3 (Peg3), Beclin 1, LC3-II, and p62 ***(32,33,64,65)*** (Fig. 1). These effects mirror that of Torin 1, a selective competitive inhibitor of mTOR ***(66)***.

Ultimately, these ECM molecules interact with their respective receptors to elicit downstream signaling pathways that converge on activating players in the core autophagic machinery including Vps34, Beclin 1, and LC3 ***(32,33,64,65,67)***. They represent a persistent, robust link between autophagy induction and angiogenic inhibition controlled by the extracellular microenvironment. A comprehensive study of these matrix proteins requires experimental treatment ranging from *in vitro* to *in vivo* models. The most powerful and effective tool for this is to clone and purify these matrix proteins in the laboratory, ensuring the user's control over the integrity, purity and quality of the protein.

The ability of certain matrix proteins to induce autophagy while inhibiting vascular growth has shown undeniable clinical promise in the identification of therapeutic targets. In the context of tumorigenesis, stimulating autophagy has been shown to be beneficial for preventing cancer development as it limits inflammation, tissue damage, and genome instability ***(68)***. These pro-autophagic matrix proteins are showing angiostatic effects in numerous cancer models, including cancer of the lung, breast, esophageal, and prostate ***(57,69,70,70-73)***. This complex interplay between tumor cells and their vascularized stroma has profound effects on cancer growth regulation ***(3,74-79)*** as angiogenic vessels exert paracrine and angiocrine modes of regulation ***(80)***. Here, we measure the effects of matrix-modulated angiogenesis through an *ex-vivo* aortic ring assay. In this assay, the outgrowth of newly formed blood vessels from the mouse thoracic aorta is indicative of a successful angiogenic process. The growing vessels recruit smooth muscle cells and pericytes to associate with the endothelial cell tube, *de facto* recapitulating the anatomy of mature blood vessels *in vivo*. Furthermore, autophagosomes can be directly observed in transgenic GFP-LC3 mice after autophagy stimulation through starvation. Protocols concerning tissue extraction for biochemical western blot analysis and mouse organ dissection for immunohistochemistry are also comprehensively detailed here.

To visualize autophagosomes, electron microscopy remains the best method to clearly depict the double-membrane structure of these vesicles because it allows to precisely distinguish ultrastructures belonging to lysosomes and other vacuoles in the cell. Over the last half-century, scientists have generated novel techniques such as confocal fluorescence microscopy and atomic force microscopy to study the autophagosomes. Immunofluorescence especially comes in handy to analyze different steps of autophagy in which autophagosomal marker proteins such as microtubule-associated light chain β (LC3β) and sequestosome-1 (p62/SQSTM1) are stained or tagged with fluorophores ***(81)***.The levels of expression of these proteins are also detectable by western blotting for further confirmation.

Although morphological analysis of autophagosomes via microscopic techniques was the key first step towards the discovery of the phenomenon of autophagy, it was not sufficient to study the functional aspect of the autophagy. In order to identify proteins as autophagic substrates, autophagosome-lysosome fusion is often inhibited via Bafilomycin A1 or chloroquine. This impedes degradation of proteins undergoing autophagy and causes a build-up of autophagosomes, both of which can be detected by western blotting or immunofluorescence ***(82)***. Ultimately, this measures autophagic flux, the measure of autophagic degradation activity, and is an effective method to study proteolytic processing of various proteins of interest.

Organelle-specific autophagy utilizes distinct molecular pathways for autophagic degradation of the target. As such, unique proteins and factors are often involved for detecting the type of "-phagy" being examined ***(83)***. In the final section, we will discuss established methods for evaluating mitophagy (mitochondrial autophagy) ***(84)*** that occurs downstream of decorin and endorepellin signaling. Mounting evidence ***(85)*** indicates mitochondrial turnover via specific autophagic processes is a paramount mechanism for mitochondrial quality control and overall cellular homeostasis.

Determining the extent of mitochondrial degradation proceeds through two primary means: imaging and biochemistry. Quantitation of mitochondrial specific chaperones residing within the mitochondrial matrix such as Hsp10, Hsp60, Hsp70; proteases such as Lon and AAA proteinases; and outer mitochondrial membrane proteins such as PTEN-induced putative kinase 1 (PINK1), adenine nucleotide translocator (ANT), and voltage-independent anion channel (VDAC1) via immunoblotting and mitochondrial DNA

(mtDNA) via qPCR are absolutely essential. Complementing mtDNA analysis is mitochondrial transcription factor A (TFAM) detection via immunoblotting as TFAM coats the mtDNA and is the sole component found in every mtDNA nucleoid ***(86,87)***. Examining oxidative phosphorylation subunits via immunoblot further reinforce accelerated mitochondrial turnover following stimulation by decorin or endorepellin. Collectively, data gleaned from both mtDNA clearance and matrix or inner mitochondrial membrane proteins are considered as strict criteria for mitophagy.

Determining the mitochondrial membrane potential gives a clear assessment of the mitochondrial permeability pore and its sensitivity to increased Ca^{2+} uptake. Mitochondrial dyes such as JC-1 are useful for measuring this property and is often a harbinger of a future mitophagic processes. There is no one singular empirical scientific methods or assays to determine, conclusively, the initiation and progression of mitophagy in mammalian cells. However, using a combination of methods, as outlined below, will give a support for this dynamic process. Therefore, we will discuss the quantification of the mtDNA and mitochondrial membrane potential determination via JC-1 staining.

2. Materials

2.1. Cloning of Recombinant Proteoglycans and Purification of His-tagged Recombinant Proteoglycans

1. Veriti 96 well thermal cycler.
2. Lysogeny broth (LB) media and LB agar plates (±100 μg/ml ampicillin). Prepare 250 ml of LB media dissolving 6.25 g of LB broth powder in 250 ml water. Prepare 500 ml LB Agar dissolving 20 g of LB broth with agar powder in 500 ml water). Autoclave liquids. Make 100 mg/ml Ampicillin stock: 0.15 g in 1.5 ml water, filter sterilized in epitube, and store at -20°C. Cool LB broth media and LB Agar and add Ampicillin (100 μg/ml). Pour Agar in 10 cm plates in the presence of a Bunsen burner (~18 ml/plate). Cool and store labeled plates at 4°C upside down to prevent condensation on agar.
3. Competent Escherichia coli cells.
4. Incubating orbital shaker.

5. Glycerol stock (50% glycerol, 50% water).
6. QIAprep Spin Miniprep Kit.
7. GeneJET gel extraction kit.
8. CutSmart buffer, Ligase buffer, T4 DNA Ligase, NheI and PmeI restriction enzymes.
9. 50X Tris-acetate-EDTA (TAE) buffer (pH 8.5): 242 g Tris base, 57.1 ml acetic acid, 100 ml 0.5 M EDTA; adjust pH to 8.5 and add water up to 1 L.
10. Agarose gel (1%). Microwave 1 or 2 g agarose in 100 ml 1X TAE (2 ml 50X TAE, 98 ml water) for 1 min for 1% and 2% gel, respectively. Wait 3 min to cool. Add 3 μl Ethidium Bromide. Pour liquid into gel mold.
11. Nanodrop 2000.
12. Short blades.
13. Human embryonic kidney cells expressing the Epstein-Barr virus nuclear antigen (HEK 293-EBNA cells).
14. OptiMEM (reduced serum with HEPES and sodium bicarbonate).
15. Lipofectamine 2000.
16. Supplemented Dulbecco's Eagle Modified Medium (DMEM): 4.5 g/L glucose, L-glutamine, and sodium pyruvate, 10% Fetal Bovine Serum (heat inactivated and filtered), 1% Penicillin/Streptomycin, 225 μg/ml G418 sulfate (with or without 2 μg/ml puromycin)
17. Hank's Balanced Salt Solution (HBSS).
18. EDTA-free proteinase inhibitor mini tablet.
19. Dialysis membrane (MWCO 6-8 kDa, Spectra/Por).
20. PEG 3350/Carbowax.
21. HisPur Ni-NTA resin beads.
22. 1X Equilibration Buffer: 20 mM Na_3PO_4, 300 mM NaCl, and 10 mM Imidazole all dissolved in phosphate buffer saline (PBS), pH 7.4.
23. 1X Binding Buffer: 25 mM Imidazole in PBS, pH 7.4.
24. 1X Elution Buffer: 250 mM Imidazole in PBS, pH 7.4.

25. 10% polyacrylamide gel: 4.796 ml water, 2.5 ml acrylamide (39:1 acrylamide/bisacrylamide, 40% solution), 2.5 ml 1.5 M Tris-HCl (pH 8.8), 0.1 ml 10% sodium dodecyl sulfate (SDS), 0.1 ml 10% ammonium persulfate (APS), 4 μl Tetramethylethylenediamine (TEMED).
26. Coomassie Brilliant Blue Dye: 450 ml methanol, 100 ml acetic acid, 450 ml distilled water, 3 g Coomassie Brilliant Blue R250; filtered.
27. Destain solution: 45% methanol, 10% acetic acid in distilled water.

2.2. Endothelial Cell Culture, Proteoglycan treatment, and Preparation of Lysate

1. Attachment factor (0.2% gelatin in PBS)
2. 12-well cell culture plates.
3. VascuLife EnGS Endothelial Medium (Lifeline Cell Technology) (see Note 1).
4. Human Umbilical Vein Endothelial Cells (HUVEC).
5. Sterile 15 ml tubes.
6. Purified recombinant proteoglycan (see Purification of His-tagged Recombinant Proteoglycan methods).
7. Sterile PBS.
8. Radioimmunoprecipitation assay (RIPA) buffer: 50 mM Tris-HCl (pH 7.5), 150 mM NaCl, 1 mM EGTA, 1 mM EDTA, 1% Triton-X 100, 0.5% sodium deoxycholate, 0.5% SDS, 1 mM Sodium orthovanadate, 1 EDTA-free protease inhibitor tablet, 1 μg/ml leupeptin, 1 μg/ml aprotinin, 100 μM TPCK, 1 mM PMSF.
9. Cell scraper.
10. 5X Sample buffer: 25 ml 1.25 M Tris-HCl (pH 6.8), 50 ml glycerol, 10 g SDS, 4 ml 0.6% bromophenol blue.

2.3. Biochemical Analysis of Autophagic Flux and Cell Signaling

1. Antibodies (Table 2).
2. Tris buffered saline (TBS) 10X: for 1L of solution, 30 g of Tris base, 80 g of sodium chloride (NaCl), 2 g potassium chloride (KCl) were dissolved in 800 ml water, stirred until the components entered the solution and the final volume was made up to 1 L.

3. Tris buffered saline tween (TBST) 1X: 100 ml of 10X TBS, 1 ml of Tween20 was dissolved in 900 ml of sterile water.
4. Blocking Buffer: 1% bovine serum albumin (BSA) (w/v) in TBST, store at room temperature.
5. Chemiluminescent substrate: SuperSignal™ west dura extended duration pico kit.
6. Transfer cassette unit: mini trans-blot cell.
7. Visualizing western blots – Image Quant LAS 4000.
8. Torin 1.
9. Chloroquine.
10. Bafilomycin A1.
11. Compound C.
12. SU5416.

2.4. Microscopic Visualization of Autophagy

2.4.1. Electron microscopy

1. Glutaraldehyde 2% (v/v).
2. Osmium tetraoxide 1% (v/v).
3. Graded ethanol (40%, 50%, 60%, 70%, 90%, 96% and 100%).
4. Embedding medium Spurr's resin (Spurr's solution: 33% resin, 66% resin and 100% resin).
5. UC7 Ultramicrotome with glass knives and diamond knives ~~(Leica)~~.
6. Toluidine Blue O stain.
7. Light microscope.
8. Copper grids.
9. Uranyl acetate (1-5% solution in water).
10. Lead citrate (0.2% of lead citrate in 0.1N sodium hydroxide).
11. JEOL 100 CX II electron microscope with Advantage HR digital CCD Camera System.

2.4.2. Atomic Force Microscopy (AFM)

1. Dimension icon AFM

2. Glutaraldehyde 2% (v/v) in HBSS: for 10 ml solution 0.2 ml of glutaraldehyde was dissolved in 10 ml HBSS (freshly prepared solution).
3. Desiccation chamber.

2.4.3. Immunofluorescence Microscopy

1. 4-chamber slides (Nunc™ Lab-Tek™ II CC2™ chamber slide system)
2. Glass cover slips (24 X 60 mm)
3. Fixative solution [4% paraformaldehyde (PFA) in PBS]: for 500 ml solution, 20 g of PFA powder was added to 400 ml of warm 1X PBS solution followed by dropwise addition of 1N NaOH solution to allow dissolution of PFA, adjust the volume of the solution to 500 ml with 1X PBS and the pH was rechecked and set to 6.9 with small amounts of hydrochloric acid, working fraction of the solution was stored at 4°C for a month and rest of the solution was aliquoted and frozen at (-20°C) for long term storage (see Note 2).
4. Permeabilization agent: 0.01% Tween20, 1% BSA in PBS (see Note 3).
5. Blocking agent: 1% BSA in PBS (see Note 4).
6. Primaries antibodies (Table 1).
7. Hard set mounting medium with DAPI (Vectashield).
8. Confocal microscope: Zeiss LSM780 NLO confocal/multiphoton microscope.
9. Fluorescence microscope: Leica upright fluorescence microscope DM5500B.

2.5. Monitoring autophagy and angiogenesis *ex vivo*

Aortic ring assay

1. 3D collagen: collagen type I rat tail (4.5 mg/ml), 199 media 10X (phenol red free), sterile water, sterile sodium bicarbonate, sterile 1M sodium hydroxide (see Note 5-6).
2. 50 ml syringes.
3. 0.22 µm filters.
4. Wild-type C57BL/6 mice.
5. Hank's balanced salt solution (HBSS).
6. 96-well plates.

7. 70% (v/v) ethanol to surface sterilize the mouse body.
8. Scalpel, sharp scissors, dissection forceps, blade, T-pins, paper towels.
9. Biohazard bag.
10. VascuLife EnGS Endothelial Medium.
11. Blocking Buffer: 2% BSA in PBS.
12. 4% PFA in PBS.
13. Lectin-1-TRITC.
14. Confocal microscope: Zeiss LSM780 NLO confocal/multiphoton microscope.
15. DAPI diluted 1:1000 in PBS.

2.7. Detecting autophagy and angiogenesis *in vivo*

2.7.1. Starvation-Induced Autophagy in GFP-LC3 Mouse Models

1. GFP-LC3 transgenic mice (Riken).
2. 500 ml 4% PFA in PBS filtered.
3. 1X PBS.
4. 500 ml 15% sucrose in PBS, made fresh each time.
5. 500 ml 30% sucrose in PBS, made fresh each time.
6. Scalpels (1 per mouse group).
7. CO_2 chamber and extra cage.
8. Liquid nitrogen in metal bucket.
9. 50 ml tubes (1 per mouse) filled with ~40 ml 4% PFA in PBS filtered.
10. Flat Styrofoam surface for dissection.
11. 28.5 gauge needles (1 per mouse).
12. Labeled 1.5 ml tubes (labeled with mouse and organ).
13. 1 tweezer.
14. 1 dissection scissor.
15. 0.5 M EDTA.

2.7.2. Mouse Tissue Extraction for Western Blot

1. Mortar and pestle.
2. Labeled pairs of tubes for each tissue sample.
3. Liquid Nitrogen in metal bucket.
4. Tissue extraction solution: In 49 ml T-PER (Tissue protein extraction reagent, Thermo Fisher) add 500 μl Halt Protease Inhibitor (100X) and 500 μl 0.5 M EDTA.
5. Nanodrop 2000.
6. 5X Sample Buffer: 25 ml 1.25 M Tris-HCl (pH 6.8), 50 ml glycerol, 10 g SDS, 4 ml 0.6% bromophenol blue.
7. 10% acrylamide gel: 4.796 ml water, 2.5 ml acrylamide (39:1 acrylamide/bisacrylamide, 40% solution), 2.5 ml 1.5 M Tris-HCl (pH 8.8), 0.1 ml 10% SDS, 0.1 ml 10% APS, 4 μl TEMED.
8. Microcentrifuge.

2.7.3. Immunohistochemistry of Tissue Angiogenic Markers

1. Optimal cutting temperature (OCT) compound.
2. Tissue mounts (Biopsy Cassettes).
3. Colorfrost Plus Microscope Slides.
4. Glass cover slips.
5. Dry ice.
6. Cryostat machine.
7. Desiccator and vacuum attachment.
8. Blocking solution: 5% BSA in PBS.
9. 1X PBS.
10. Vertical glass slide container.
11. Hard set mounting medium with DAPI (Vectashield).

2.8. Monitoring Mitophagy

2.8.1. Mitochondrial DNA determination

1. RNAzol B.
2. Extraction Buffer (EB): 4 M guanidine thiocyanate, 50 mM sodium citrate, and 1 M Tris-free base.
3. Polyacryl carrier.
4. Chloroform.
5. Isopropanol.
6. 8 mM NaOH.
7. 1 M Hepes.
8. 100 mM EDTA, pH 8.0.
9. 75% ethanol.
10. 1 x PBS, pH 7.4.
11. 6-well plastic cell culture plates.
12. PBS.
13. Decorin / endorepellin.

2.8.2. Detection of mitochondrial membrane permeability via JC-1 staining

1. Attachment Factor (0.2% Gelatin in PBS)
2. 4-chamber glass slides.
3. 7.5 mM JC-1 stock solution.
4. Leica upright fluorescence microscope DM5500B.

3. Methods

3.1. Cloning of Recombinant Proteoglycans and Protein Core Fragments

To monitor matrix-induced autophagy, an optimal experimental strategy involves cloning, synthesizing, and purifying recombinant proteoglycans and protein core fragments in the laboratory. This ensures high purity in the process of protein preparation that is not otherwise available by purchasing

proteoglycans from industrial resources. Here, we provide a detailed protocol of the entire process, from cloning the recombinant proteoglycan cDNA into the expression vector to transfecting eukaryotic HEK 293-EBNA cells with the foreign plasmid to purifying the secreted recombinant protein from cell media. In particular, we chose the pCEP-Pu (derivative of pCEP4) expression vector containing a BM40 secretion sequence upstream of the cDNA insertion site ***(54)***. This ensures secretion of the recombinant proteoglycan into the media for effective purification.

1. The full cDNA coding sequence of the proteoglycan region of interest was constructed with a preceding NheI restriction site (GCTAGC) and proceeding with nucleotides encoding for 6 histidine residues followed by the PmeI restriction site (GTTTAAACG) (see Note 7).
2. This cDNA was then cloned into pUC57 (Amp^R) (see Note 8).
3. The pUC57 containing the cDNA (pUC57-cDNA) and the empty pCEP-Pu vector were transformed into competent E. coli cells. For this purpose, 25 μl competent cells were mixed with 20 ng DNA and incubated for 30 min on ice. The solution was then incubated at 42˚C for 45 sec and put back on ice for 2 min. In each transformation, 475 μl warmed LB media (no Ampicillin added) was added and placed in a shaker at 37˚C for 1 h.
4. A portion (20 μl) of each transformed solution was then aliquoted into separate tubes to make 3 dilutions in LB media (1:10, 1:100, and 1:000 with negative control). In sterile conditions, each dilution was plated in agar plates containing 100 μg/ml ampicillin and incubated at 37˚C overnight (see Note 9).
5. Two colonies were suspended separately in 2 ml broth containing 100 μg/ml ampicillin and placed in 37˚C shaking for 6-8 h.
6. In a separate tube, 500 μl of bacteria culture was suspended with 500 μl glycerol stock. The remaining 1.5 ml was spun down at 8,000 rpm for 10 min and stored at -20˚C for future plasmid purification.
7. Plasmids from cells transformed with pUC57-cDNA and pCEP-Pu were purified from transformed E. coli using the QIAprep Spin Miniprep kit.

8. pUC57-cDNA and pCEP-Pu plasmid underwent double digest with NheI and PmeI. The following was added in a PCR tube: 1 μg plasmid, 5 μg Cutsmart Buffer, 1 μg NheI, 1 μg PmeI, and 42 μg water. The solutions were subjected to the following conditions: 37˚C (2-3 h), 65˚C (20 min), and stored at 4˚C.
9. The uncut and double digested plasmids were run on a 1% agarose gel with ethidium bromide at 110V alongside a 1 kb ladder (see Note 10).
10. The linearized pCEP-Pu plasmid and cDNA fragment were cut out of the gel under UV light with short blades and extracted using GeneJET gel extraction kit (Thermo Fisher) (see Note 11).
11. The DNA concentration of the extraction was measured via Nanodrop (see Note 12), and a 10:1 (vector:insert) ratio solution of 75 ng total DNA was made for ligation (see Note 13).
12. Double digested pCEP-Pu and cDNA were then ligated together. The following was added in a PCR tube: 50 ng cDNA insert, 25 ng pCEP-Pu vector, 2 μl ligase buffer, 1 μl ligase, and water up to 20 μl. The reaction mixture was subjected to the following conditions: 16˚C (16 h), 65˚C (10 min), and stored at 4˚C.
13. Ligated pCEP-Pu-cDNA were transformed into competent E. coli cells using 5 ng ligated plasmid, selected against ampicillin, grown in culture overnight, and purified (see step 3-4) (see Note 14).
14. Using appropriate primers (see Note 15), the cDNA was sequenced and ligated regions of the plasmid to confirm in-frame and correct nucleotide sequence.
15. pCEP-Pu-cDNA were stably transfected into HEK 293-EBNA cells. HEK 293-EBNA cells were grown in 10 cm dish at 37˚C in supplemented Dulbecco's Modified Eagle Medium (DMEM) until 70-80% confluent (see Note 16). Two tubes were labeled lipofectamine and DNA and the following were added. Lipofectamine tube: 500 μl OptiMEM media, 30 μl lipofectamine 2000. DNA tube: 500 μl OptiMEM media, 10 μg plasmid.
16. Tubes were incubated for 5 min in room temperature.
17. Contents from the 2 tubes were mixed together and incubated for 45 min at room temperature.

18. Media from cells were aspirated and 5 ml OptiMEM with DNA-lipofectamine mixture was added gently to cells for 6 h at 37˚C (see Note 17).
19. OptiMEM was aspirated and replaced with 10 ml pre-warmed supplemented DMEM overnight.
20. Media was changed again with supplemented DMEM.
21. After 48 h of transfection, add supplemented DMEM with 500 ng/ml puromycin (see Note 18) and grow in puromycin until stable colonies propagate.
22. Maintain stably transfected cell lines in supplemented DMEM with 2 μg/ml puromycin.

Purification of His-tagged Recombinant Proteoglycans

23. HEK 293-EBNA cells transfected with pCEP-Pu-cDNA were propagated until 80-90% confluent (see Note 19).
24. Media from the cells were aspirated and cells were washed with serum-free HBSS.
25. Cells were serum-starved with serum-free supplemented DMEM media with 2 μg/ml puromycin for 72 h at 37˚C (see Note 20).
26. Media was filtered in a 0.22 mM filter, and a single EDTA-free protease inhibitor mini-tablet was dissolved in the media by rocking in room temperature (see Note 21).
27. Filtered media was transferred to a Spectra/Por 2 Dialysis membrane and concentrated with PEG/Carbowax to ~30 ml (see Note 22).
28. Media was dialyzed in 2 L sterile water with 0.1 mM Phenylmethylsulfonyl fluoride (PMSF) spinning at 4˚C for 36 h (see Note 23).
29. Media was dialyzed in 2 L Binding Buffer with 0.1 mM PMSF for 36 h (see Note 23).
30. An aliquot of 500 μl HisPur Ni-NTA resin beads were pipetted to an open column (see Note 24).
31. An aliquot of 2 ml Equilibration Buffer then 2 ml Binding Buffer were run through the column (see Note 25). Flow-through was discarded.
32. The dialysate was run through the column 1-3 times, and the unbound flow-through was saved.
33. An aliquot of 4 ml Binding Buffer was run through the column.

34. An aliquot of 10 ml Elution Buffer was run through the column and 20 fractions of 500 μl were numbered and collected (see Note 26).
35. A small aliquot of 2-5 μl per fraction was run on a 10% polyacrylamide gel and stained with Coomassie dye for 20-30 min, then washed in Destain solution for 36 h.
36. Fractions containing recombinant protein were pooled together. The concentration of the purified protein was measured by running electrophoresis with 1 and 2 μl of eluted protein with BSA standards (0.25, 0.5, 1, and 2 μg) (Fig. 2).
37. Optional: To further concentrate final concentration of purified protein, PEG was used for 10-15 min.

3.2. Endothelial Cell Culture, Proteoglycan treatment, and Preparation of Lysate

1. Approximately 300 μl 0.2% gelatin was incubated in 12-well plates (~4 cm^2/well) in 37˚C for at least 2 h.
2. After excess gelatin was aspirated, gelatinized 12-well plates were placed under UV light in a laminar flow hood for 10-20 min.
3. Each well was seeded with ~5 x 10^4 human umbilical vein endothelial cells (HUVEC) in pre-warmed supplemented VascuLife EnGS Endothelial Medium. Pre-warmed media were replenished every 2 days until cells were grown to confluency (see Note 27).
4. After cells had been confluent for 1-2 days (see Note 28), experimental treatments were initiated. In a sterile 15 ml tube, purified recombinant proteoglycan (200 nM) was added to cell media (500 μl/well), and the solution was incubated at 37˚C for 30 min.
5. Media from cells were aspirated, and pre-warmed proteoglycan treatments were added to wells (500 μl/well) and incubated at 37˚C for the designated time period (see Note 29).
6. Post-treatment, cell culture plates were placed on ice, and media were aspirated from wells. Using ice-cold 1X PBS, cells were washed once, and RIPA (200 μl/well) was added for 10-15 min (on ice at room temperature, rocking).

7. Cells were manually scraped on ice. Remaining lysates from each well were vortexed in 50 μl 5X Sample Buffer, boiled for 2 min, and stored in -20˚C for western blot analysis (see Note 30).

3.3 *In vitro* Biochemical Analysis of Matrix-Induced Autophagy

Autophagic Flux & Cell Signaling Assay

Proteoglycans such as decorin protein core and the C-terminal perlecan fragment endorepellin have been shown to activate autophagy through inducing phosphorylation of AMPKα ***(65,88)***. Further, canonical activation of AMPKα via phosphorylation at Thr172 in the T-loop region occurs physiologically upon nutrient deprivation and inhibits mTOR activity to activate autophagy ***(89,90)***.

1. Endothelial cells were seeded and cultured appropriately (see method 3.2, steps 1-5).
2. Endothelial cells were treated with the recombinant proteoglycan ±the following signaling/flux inhibitors: Bafilomycin A1 (500 nM) or Chloroquine (20 μM), inhibits autophagosome-lysosome fusion. Compound C (1 μM), inhibits activation of AMPKα. Torin 1 (20 nM), selectively inhibits mTOR. SU5416 (30 μM), VEGFR1/2 tyrosine kinase inhibitor.
3. Cells were lysed and processed for western blot analysis (see Section 3.2, steps 6-7).
4. After samples were run through an acrylamide gel and transferred onto a nitrocellulose membrane, membranes were blocked in 1% BSA in TBST, rocking for 1 h at RT.
5. Membranes were incubated overnight in primary antibodies, diluted at 1:1000 in 1% BSA in TBST (see Note 31) (see Table 1).
6. Once the primary antibody was removed the following day, membrane was washed three times in TBST (15 min each).
7. Secondary antibody was added, diluted at 1:4000 for 1 h at RT and washed with TBST thereafter for three times (15 min each).
8. Membrane was treated with chemiluminescent substrate for 2 min and visualized using an ImageQuant machine.

3.4. Microscopic Visualization of Autophagy

3.4.1. Electron Microscopy (EM)

1. Specimens were fixed in 2% glutaraldehyde (GA) in 0.1 M PBS at RT for 4 h.
2. After GA fixation, specimens were fixed in 1% osmium tetroxide (OT) in 0.1 M PBS at 4°C for 2 h.
3. Post-fixation tissue fragments were dehydrated in a gradient of ethanol solutions (40%, 50%, 60%, 70%, 80%, 90%, 96% and 100%).
4. Tissue fragments were embedded in plastic resin (Spurr's solution: 33% resin, 66% resin and 100% resin) and polymerized overnight at 80°C.
5. The fix and embedded tissue fragments were cut into 0.5-1 micron thick sections using UC7 ultramicrotome with glass knife. Sections were then transferred to glass microscope slides, stained with Toluidine Blue O stain, and observed under a light microscope to check the morphology of the tissue.
6. After visually confirming the intactness of morphological integrity of the tissue fragment, sections were further cut into 100-120 nm thick sections using UC7 ultramicrotome using a diamond knife.
7. Sections were collected on copper grid and stained with uranyl acetate and lead citrate. Briefly, a small petri was placed within a big petri making two chambers. A small petri dish was covered with parafilm and the outer zone filled with 10-15 NaOH pellets. Big droplets of uranyl acetate were put onto the parafilm (covering the smaller petri) with number of droplets corresponding to number of copper grids to be stained. The copper grids were upturned with sample facing the drops and left for 15 min to allow uptake of stain. The grids were removed, dried on paper and sequentially washed three times in distilled water. The same process was repeated for lead citrate in a similar but separate setup.
8. Thick sections of 100 nm were observed using a JEOL electron microscope. Digital images were created using an Advantage HR Digital CCD camera system that was attached to the electron microscope.

3.4.2. Atomic Force Microscopy (AFM)

1. HUVEC were grown to confluency on attachment factor coated four-chamber slides.
2. Cells were washed with ice-cold PBS 1X and fixed in 2% glutaraldehyde diluted in HBSS.
3. Fixed cells were re-washed with PBS 1X and dried in desiccation chamber.
4. Cell structure was obtained by probing fixed cells in tapping mode using a nano-sized silicon tip (tip radius R ~ 10 nm, spring constant ~42 N/m, NCHV-A, BrukerNano).
5. To measure the elasticity modulus of cells, they were grown up to confluency and probed without fixing.
6. An optical microscope was used to locate individual cells before performing nano-indentation at 7 μm/s indentation depth rate using a microspherical tip (R ≈ 2.5 μm, k ≈ 0.1 N/m) in the same media in which cells were grown (Dimension Icon AFM) (see Note 32).
7. The force-depth loading curve obtained from nano-indentation was fit using Hertz model with the finite cell height correction, and the effective elasticity indentation modulus was calculated. The Poisson's ratio of the cells was set to 0.5.

3.4.3. Immunofluorescence Microscopy

1. 5 X 10^5 HUVEC cells were plated on attachment-factor coated 4-chamber slide and grown to confluency.
2. The cells were washed with 1X PBS twice and fixed using 100 μl of 4% PFA per well while on ice for 20 min.
3. The PFA was aspirated, and cells were washed again with 1X PBS (see Note 33).
4. 100 μl of the Permeabilization Buffer was added to each well and rocked for 30 s before washing off the buffer.
5. The cells were blocked with 100 μl 1% BSA for 45 min at RT.
6. Primary antibodies were diluted at 1:200 ratio in 1% BSA solution in PBS and added 200 μl per well for 1 h (Table 1).
7. The cells were washed thrice with 1X PBS for 5 min each.

8. Secondary antibodies were diluted at 1:400 in 1% BSA solution in PBS and added 200 µl per well for 1 h (Table 1).
9. The cells were then washed thrice with 1X PBS for 5 min each.
10. PBS was aspirated, and the walls of the slide were removed with a separator.
11. The slide was dried to evaporate excess PBS, and two drops mounting media containing DAPI was added per well before overlaying slide with cover slip.
12. The corners of the slide were sealed with clear nail-polish and allowed to air dry for 2 h before visualization.
13. The slide was viewed at 63X using Zeiss Confocal Microscope or Leica Fluorescence Microscope.

3.6. Monitoring autophagy and angiogenesis *ex vivo*

3.6.1. Aortic ring assay

Aortae can be taken from wild-type C57BL/6 mice. Using a purified pro-autophagic matrix protein, aortic rings induced with protracted autophagy showed reduced sprouting, indicative of hindered angiogenesis, while control rings grew proficiently (Fig. 4).

3D collagen preparation for embedding aortic rings

1. The following were added to a 1.5 ml tube on ice to form the 3D collagen gel mixture: 350 µl of collagen, 320 µl of autoclaved water, 120 µl of 199 media 10X, 280 µl of $NaHCO_3$ and 20 µl of NaOH (see Note 34-35).
2. Aliquots of 50 µl from the mixture were added to each well of a 96-well plate (see Note 36) and place in a 37°C incubator for 30 min to allow polymerization of collagen gel layer 1.
3. For collagen gel layer 2, a separate 3D collagen gel mixture was made (see method 3.6.1, step 1) and kept on ice.

Dissecting and preparing aortic rings

4. The heart and lungs of the euthanized mouse were removed to expose the aorta (see Note 37). The aorta will appear as a fatty-white tube which runs down from the neck region to the diaphragm along the spine.
5. Using a pair of forceps, the thoracic end of the aorta was stabilized and the abdominal end was cut. The aorta was detached from the spine by running a scalpel gently up towards the thoracic end of the aorta where it branches into brachiocephalic artery, left carotid and left subclavian arteries.
6. The anterior end of the aorta was cut to release the dissected aorta (see Note 38).
7. The aorta was transferred onto a petri dish on the dissection board and immersed in HBSS.
8. Using a dissection microscope, the morphology of the aorta was verified (see Note 39). Visceral fat was removed around the aorta using a sharp blade.
9. The aorta was cut into small, uniform rings ~0.5 mm in width.

Embedding aortic rings into collagen type I and allowing sprouting

10. Aortic rings were placed one at a time in each well of the 96-well plate layered with 3D collagen (see method 3.6.1 step 1).
11. After placing the rings, a second layer of 50 µl collagen gel was added and incubated at 37°C for 30 min (see method 3.6.1 step 3).
12. An aliquot of 100 µl HUVEC VascuLife EnGS endothelial medium was added to each well and the 96-well plate was placed back into the incubator.
13. The 96-well plate was monitored every day to visualize sprouting.
14. When vessels began to sprout from the aortic rings, the purified recombinant matrix protein was added to the surrounding media at the appropriate functional concentration (ex: 200 nM endorepellin). As a control, an equal amount of PBS was added to the media of a separate aortic ring.

Staining aortic rings with lectin and DAPI to visualize sprouting

15. The culture media was removed and the aortic rings were washed with HBSS.
16. Rings were fixed in 100 µl of 4% PFA per well for 2 h rocking in RT.

17. The PFA was aspirated and rings were washed with PBS (see Note 40).
18. Rings were blocked with 2% BSA in PBS for 3 h at RT (see Note 41).
19. Rings were incubated for 3 h at RT (dark) in a 1:200 dilution of lectin-1-TRITC in Blocking Buffer to stain the endothelial cells.
20. Rings were washed 3 times in PBS for 15 min each.
21. Rings were stained with DAPI (1:1000) for 10 min (dark)
22. Rings were washed 3 times with PBS for 15 min each (see Note 42).

Visualization of the rings

23. The 96-well plate was taken to the confocal facility and visualized with 63X oil objective.
24. Zen black software was used to acquire z-stack images.
25. Image J software was used for 3D reconstruction of images acquired with Zen black. Individual slices of z-stack were converted into a stack and then into maximum intensity projection image.

3.7. Detecting autophagy and tumor angiogenesis *in vivo*

3.7.1. Starvation-Induced Autophagy in GFP-LC3 Mouse Models

1. From the same cage, an equal number of GFP-LC3 mice were randomly separated into two cages, one for each group (fed vs fasted).
2. Starting early in the morning (7-8 AM), food sources from each cage was removed for 25 h. Water supplies were maintained to prevent dehydration.
3. Mice were immediately euthanized and dissected for biochemical and IHC analysis (see below).

Mouse Organ Dissection & Biochemistry

1. One at a time, mice were euthanized in a CO_2 chamber and cervical dislocation was performed.
2. Blood was extracted as follows. The mouse abdomen, peritoneum, and chest cavity are cut open with beating heart exposed. Using a syringe, blood was extracted from heart and transferred to tube precoated with 0.5 M EDTA overnight. Tubes were centrifuged at 2000 rpm for 10 min at 4˚C, and serum (supernatant) was transferred into a fresh tube using glass pipettes.

3. Organs were extracted (heart, lungs, kidney, liver, tumor). Organs were removed and briefly rinsed in PBS. A small piece of each organ was cut and placed in 4% PFA for IHC. Remaining part was placed in a 1.5 ml tube and flash frozen in liquid nitrogen and stored in -80˚C for protein extraction (see method 3.7.3). Rock organs in PFA for 4 h at room temperature (RT). Organs were incubated in 15% sucrose at RT, rocking for 4 h. Organs were incubated in 30% sucrose at RT, rocking overnight.

3.7.3. Mouse Tissue Extraction for Western Blot

1. Tubes with frozen tissue were kept in liquid nitrogen throughout extraction.
2. For each tissue sample: Liquid nitrogen was poured into a mortar and pestle to pre-cool. Tissue was crushed with pestle while submerged in liquid nitrogen (see Note 43). Remaining tissue was stored back in -80˚C. Crushed tissue was poured into new labeled tube carefully (cover opening of tube partially with finger to prevent tissue from coming out when liquid nitrogen evaporated). An aliquot of 1 ml tissue extraction solution was added to tube and vortex thoroughly. Mortar and pestle were wiped down with dry paper towel for next tissue.
3. Samples were vortexed thoroughly again (~30 sec) and centrifuged at 10,000 rpm for 8-10 min at 4˚C.
4. Supernatant was transferred into new labeled tube, and pellet was discarded.
5. Using the Protein A280 program in the Nanodrop, protein concentration of each sample was measured and volumes for 30 μg were calculated.
6. In separately labeled tubes, 30 μg of each sample was aliquoted with the appropriate amount of 5X Sample Buffer, adding water as necessary to normalize volumes.
7. Tubes were boiled for 2 min and run on a 1.5 mm 10% acrylamide gel, transferred, and probed with the appropriate antibodies (see Note 44).
8. Remaining samples were stored at -80˚C.

3.7.3. Immunohistochemistry of Tissue Angiogenic Markers

3.7.4.1. Mounting tissue in OCT:

1. Organs were transferred from sucrose to a dry paper towel
2. Small parts of each organ were cut and the rest put back in 4% PFA for long-term storage at 4˚C.
3. OCT was poured carefully onto labeled tissue mount (see Note 45).
4. Organs were placed in OCT, and more OCT was added to submerge organs (see Note 46).
5. Tissue blocks are placed carefully in -20°C to solidify OCT and stored at -20°C (see Note 47).

Cutting tissue sections onto slides

6. Approximately 10 glass slides were numbered and labeled per tissue mount.
7. Solidified tissue mounts were placed on dry ice for transportation to cryostat.
8. All tissue mounts were incubated in the -20°C cryostat for 5-10 min to equilibrate.
9. The plastic top of the tissue mount was removed.
10. OCT was dispensed on head of the cryostat chuck and the head of the tissue mount was stabilized on the chuck (see Note 48).
11. Chuck was tightened onto the cryostat sectioning interface.
12. Tissue sections were cut at 8-10 μm (see Note 49).
13. Slides were placed in a vacuum-tight desiccator at RT for 1 h to dry, then stored at -80°C for future IHC.

Staining slides for IHC

14. Slides were blocked in 5% BSA in PBS for 1 h, RT (see Note 50).
15. Excess liquid was dried off the slide using a paper towel without disrupting the tissue section.
16. Tissue sections were submerged with primary antibody solution (in 5% BSA in PBS) for 1 h in RT (see Note 51) (Table 2).
17. Slides were carefully washed 3 times in PBS.
18. Tissue sections were submerged with secondary antibody solution (in 5% BSA in PBS) for 1 h in RT (see Note 51) (Table 2).

19. Slides were carefully washed 3 times in PBS.
20. DAPI hard mount was applied to each section (1 drop/section), the cover slip was placed over sections, and clear nail polish was applied to the corners. Slides were stored at 4°C in the dark.

3.8. Mitophagy Monitoring

3.8.1. Mitochondrial DNA isolation and determination

Determining mitochondrial membrane polarization ($\Delta\Psi m$) proceeds via live cell staining with the JC-1 vital dye. Mechanistically, JC-1 is a lipophilic cationic dye sensitive to voltage fluctuations. JC-1 accumulates in the inner mitochondrial membrane in response to $\Delta\Psi m$. A low $\Delta\Psi m$ denotes loss of membrane potential, JC-1 is monomeric and exhibits green fluorescence. However, under conditions of health $\Delta\Psi m$, JC-1 accumulates proportionately to the $\Delta\Psi m$ and forms JC-1 aggregates, shifting the JC-1 emission spectrum towards a red fluorescence ***(91)***.This can be quantified using ImageJ software.

1. Sub-confluent (~75-80%) tumor cells, seeded in 6-well dishes, were treated with 200 nM purified decorin at 37°C.
2. The 6-well dish was gently placed on ice and washed once with ice-cold PBS.
3. A volume of 1 ml of RNAzol B was added to each well and pipetted up and down several times to homogenize cells. The homogenate was transferred to a clean 2.5 ml round bottom centrifuge tube and place on ice. The wells were washed with an additional 1 ml of RNAzol B and transferred to the appropriate 2.5 ml tube.
4. An aliquot of 100 μl chloroform for every 1 ml of RNAzol B was added and the mixture was vortexed at maximum speed for 20 s. The tubes were incubated for 5 min at RT.
5. The tubes were centrifuged (12,000xg) for 15 minutes at RT. The RNA-containing aqueous top layer was discarded (see Note 52).
6. An aliquot of 500 μl EB for every 1 ml of RNAzol B was added to the remaining interphase and organic phase layers. The tubes were inverted 6-7 times and incubated at RT for 10 min.

7. The tubes were centrifuged (3000xg) for 30 min at 4°C and the upper layer containing genomic DNA and mitochondrial DNA was transferred to newly labeled 1 ml tubes.
8. An aliquot of polyacryl carrier (4 μl for every 1 ml of RNAzol B used) was added followed by the addition of isopropanol (400 μl for every 1 ml of RNAzol B used) to precipitate the DNA species. The tubes were inverted 6-7 times and incubated at RT for 10 min.
9. Tubes were centrifuged (12,000xg) for 5 min at 4°C. Supernatant was discarded. The remaining pellet was washed with 1 ml 75% ethanol and incubated at RT for 5 minutes. Tubes were inverted 6-7 times to dislodge the pellet from the bottom of the tube and centrifuged (12,000xg) for 5 min at 4°C. The supernatant was discarded. This step was repeated four times to ensure proper washing of the DNA pellet.
10. The pellet was air dried at RT for 5 min to remove residual ethanol (see Note 53).
11. An aliquot of 30 μl 8 mM NaOH was added to dissolve the DNA pellet followed by centrifugation (12,000xg) for 10 min at 4°C to remove any undissolved material.
12. The supernatant (~30 μl) was transferred to a freshly labeled 200 μL tube. An aliquot of 0.5 μl 1 M Hepes solution was added to bring sample pH to 8 followed by 0.5 μl 100 mM EDTA. This was vortexed for 15 s. The isolated genomic DNA/mitochondrial DNA (gDNA/mtDNA) mixture was stored at either 4°C or -20°C. Repeated freeze/thaw cycles should be avoided.
13. Using 10 ng of freshly isolated DNA per reaction, conventional qPCR was conducted using the following primer sequences (see Note 54): Primer sequences for mtDNA detection of a 0.2Kb fragment of the ND1 gene: Forward: 5'-CCCATTCGCGTTATTCTT-3' / Reverse: 5'-AAGTTGATCGTAACGGAA-3'. Primer sequences for gDNA detection of a 0.2Kb fragment of the LPL gene: Forward: 5'-GGATGGACGGTAAGAGTGATT-3' / Reverse: 5'-ATCCCAGGGTAGCAGACAGGT-3'.

3.8.2. Detection of mitochondrial membrane permeability via JC-1 staining

1. The desired number of 4-chamber glass slides were gelatinized with 200 μl 0.1% gelatin for 3 h at 37°C. Gelatin was aspirated, and plates were dried under UV-A/B for 30 min.
2. Endothelial or tumor cells were grown to confluency and treated with 200 nM decorin or 200 nM endorepellin for desired amount of time 37°C (see Note 55).
3. Cells were incubated with 7.5 μM JC-1 for 20 min at 37°C, then gently washed 3 times in warm PBS. Add 500 ml of warmed cell-type appropriate media.
4. Live cells were imaged using Leica upright fluorescence microscope DM5500B.

Notes

1. Always add 1% Penicillin/Streptomycin to cell media
2. Paraformaldehyde powder is very corrosive to skin and should be handled wearing gloves, once it's added to warm 1X PBS it gets volatile and should be worked with a mask-on.
3. Cells should be directly transferred from the incubator to the AFM machine, not be allowed to stand out of the incubator for more than 30 min, this compromises with their buffering ability and induces stress in them.
4. BSA powder is temperature sensitive and should be stored at 4°C always.
5. Collagen type I rat-tail can be a little turbid but that doesn't affect its functionality. Keep the collagen cocktail (mixture of all the components like bases, media and collagen) on ice to avoid rapid polymerization in the falcon tube itself. Ice helps to allow transfer of collagen gel to 96-well plates while still in its liquid state.
6. 199 media should be phenol red-free to allow visualization of pH change (color change from yellow to red) on addition of bases (NaOH and $NaHCO_3$) to the collagen. Rat tail collagen I is acidic to begin with since it has been extracted using acetic acid, adding bases allows polymerization of the collagen into gel form. Change in pH should be visible to eliminate any errors in collagen polymerization.

7. Verify that cDNA sequence contains no NheI or PmeI restriction sites. Extra nucleotides may be added to ensure that the cDNA sequence will be in-frame once inserted into the pCEP-Pu vector.
8. Genscript offers gene synthesis of custom cDNA sequences into pUC57 (Amp^R) vectors.
9. Place agar plates upside down in the incubator to prevent condensation on the agar.
10. Run the gel longer to obtain greater separation of bands.
11. Elute DNA from gel with water to obtain a lower salt solution.
12. Aim for a DNA concentration of 5-20 ng/μl and ~2 260/280 ratio.
13. Calculating molar ratio of 10:1 (vector : insert) with 75 ng total DNA:
    - Ex: vector/insert = 10 kb/2 kb = 5
    - Multiplication factor to obtain 10:1 = 10/5 = 2
    - Vector = 25 ng
    - Insert = 25 x 2 = 50 ng
14. In miniprep extraction, elute with EB buffer.
15. Design sequencing primers with the following criteria:
    - Melting temperature (Tm) range of 50-65˚C
    - Cannot dimerize
    - Between 18-30 bp in length
    - GC content of 40-60%
16. Grow HEK 293-EBNA cells in culture for 2 passages before transfection.
17. Ensure that handling of lipofectamine and HEK 293-EBNA cells are entirely sterile to avoid contamination in transfection.
18. Expect to see a lot of cell death upon puromycin addition. This ensures stable transfection.
19. Increased confluency is recommended for optimal protein secretion.
20. Cells may be serum starved for 3-5 days for optimal protein yield.
21. For long-term storage, store in -80˚C.

22. Dialysis membrane with a lower MWCO is recommended for faster concentration (6-8 kDa recommended).
23. Change dialysis solution once after 12-24 h for optimal dialysis.
24. Use a 1 ml pipette with the pipette tip cut slightly to prevent damaging resin beads.
25. Use glass pipettes to transfer all liquid into column to prevent protein adherence.
26. An aliquot of 500 μl is approximately 10 drops.
27. Grow cells in 1 ml media per well in 12-well plate.
28. Wait at least 1 day after cells reach confluency before starting the appropriate treatment. This allows time for cells to fully lay down their basement membrane and extracellular matrix.
29. Generally, recombinant proteoglycan treatments do not extend beyond 24 h due to protein degradation.
30. In preparation for western blot analysis, measuring the protein concentration of each lysate is generally not necessary since all samples came from fully confluent monolayers of endothelial cells.
31. Membrane can also be blocked in BSA overnight and then treated with primary antibody the following day for 3 hours, followed by washing and treating with secondary antibody for 1 h. This step can be optimized depending on the antibody company/quality.
32. After fixing the cells, they can be stored at 4°C for 4-5 days until staining.
33. Use glass pipettes to transfer all liquid into column to prevent protein adherence.
34. It is essential that the constituents of the 3D collagen cocktail are added in the sequence mentioned in the methods section, with bases being added at the end, to allow commencement of polymerization after addition of all the components. Bases make the collagen (which is acidic to begin with) into neutral constituency thus providing suitable conditions to begin polymerization.
35. 3D collagen cocktail constituents should be thoroughly mixed to allow uniform polymerization across the volume and homogenous texture of the gel.

36. 96-well plate is ideal for aortic ring assay since bigger well-size plates cause diffusion of growth factors thereby hindering sprouting.
37. Upon cutting the heart blood will spurt out of the vessels filling up the cavity. Use paper towels to soak the blood.
38. Aorta tends to curl up when the second end is cut (anterior end). Overlay the aorta with few drops of HBSS to smoothen out the tube, after placing it on the dissection board.
39. Esophagus of the mouse also runs close to the aorta and may be mistaken for aorta. Aorta appears as hollow white tube with fat around it, while esophagus is pinker in appearance with very small lumen.
40. Rings can be stored in PBS after fixing with PFA for 1 week until they are stained with antibodies/dyes.
41. Permeabilization of aortic rings was skipped since they were only stained with lectin-1-TRITC dye, which recognizes glycoproteins present in the basal membrane of endothelial cells. If the rings are to be probed for any intracellular protein, they should be permeabilized with tween which is added to PBS in which BSA is dissolved in the blocking step.
42. Rings should be visualized within 1-2 days of staining with lectin-1 and DAPI to avoid diffusion of signal and development of contamination. For long term storage (up to 1 month), sodium azide can be added to the wells in very low quantity.
43. Make sure to work quickly throughout and triple glove to protect hands from liquid nitrogen.
44. Avoid using mouse antibodies to probe mouse tissue to avoid nonspecific signal.
45. Avoid bubbles in OCT that interferes with cutting sections. Dispense OCT conservatively to keep in the boundary of the tissue mount. Label tissue mount appropriately for each organ or mouse type.
46. Keep organs in the same plane when embedding in OCT for easy sectioning.
47. For long term storage, keep tissue mounts at -80°C.
48. Let OCT cool on chuck for ~30 sec before attaching tissue mount for better adhesion.

49. Initially, set section thickness to 20 μm until tissue in OCT is reached, then readjust to 8 μm for actual tissue section. Use brush to flatten section as it is being cut, then touch room temperature slide to OCT section and place in slide holder in RT. Depending on the surface area of the tissue section, two tissue sections can be placed on each slide.
50. For washing and blocking, use vertical glass chambers filled with solution that can hold multiple slides for better efficiency.
51. For neater immunostaining, use a wax pencil to draw a circular boundary around the tissue section on the slide.
52. Instead of discarding the aqueous RNA phase, RNA can be isolated from this phase to verify target RNA levels. For example, if a protein has been implicated in mitophagy, one can knockdown the target protein via RNAi techniques and verify depletion via the target RNA in the same samples being assayed for mtDNA content.
53. An alternative to air drying for 5 minutes, a KimWipe (or sterile Q-tip) can be used to remove the residual ethanol. Great care must be taken to avoid adsorption of the pellet to the KimWipe or Q-tip.
54. Primer stock concentration are at 100 μM and utilized at a working concentration of 10 μM. Calculate fold changes according to the comparative $\Delta\Delta C_T$ method using the gDNA C_T values as calibrator samples. As an alternative to mtDNA quantification via the comparative $\Delta\Delta C_T$ method, establishing a standard curve of known gDNA concentrations can be used to calculate absolute copy numbers of the mtDNA per condition.
55. It is strongly encouraged to run a positive control for the JC-1 staining. Known protonophores such as carbonyl cyanide-*m*-chlorophenylhydrazine (CCCP) or carbonyl cyanide-*p*-trifluoromethoxy-phenylhydrazone (FCCP). It is recommended to use CCCP at 30 μM and FCCP at 500 nM for either 1 h or 15 minutes, respectively.

Acknowledgements

The authors would like also to thank Thomas Neill and Simone Buraschi for their invaluable scientific contributions and suggestions. This work was in part supported by NIH grants CA39481 and CA47282 to RVI. Carolyn Chen is a recipient of the NIH training grant T32 AR052273.

References

1. Zollinger AJ, Smith M.L. (2017) Fibronectin, the extracellular glue. Matrix Biol 60-61**:** 27-37

2. Komorowicz E, Balazs N., Varga Z., Szabo L., Bota A., Kolev K. (2017) Hyaluronic acid decreases the mechanical stability, but increases the lytic resistance of fibrin matrices. Matrix Biol 63**:** 55-68

3. Tolg C, Yuan H., Flynn S.M., Basu K., Ma J., Tse K.C.K., Kowalska B., Vulkanesku D., Cowman M.K., McCarthy J.B., Turley E.A. (2017) Hyaluronan modulates growth factor induced mammary gland branching in a size dependent manner. Matrix Biol 63**:** 117-132

4. Ringer P, Colo G., Fassler R., Grashoff C. (2017) Sensing the mechano-chemical properties of the extracellular matrix. Matrix Biol. 64**:** 6-16

5. Wilson SE, Marino G.K., Torricelli A.A.M., Medeiros C.S. (2017) Injury and defective regeneration of the epithelial basement membrane in corneal fibrosis: A paradigm for fibrosis in other organs? Matrix Biol. 64**:** 17-26

6. Di Russo J., Hannocks M.J., Luik A.L., Song J., Zhang X., Yousif L., Aspite G., Hallmann R., Sorokin L. (2017) Vascular laminins in physiology and pathology. Matrix Biol 57-58**:** 140-148

7. Miller RT (2017) Mechanical properties of basement membrane in health and disease. Matrix Biol 57-58**:** 366-373

8. Pozzi A, Yurchenco P.D., Iozzo R.V. (2017) The nature and biology of basement membranes. Matrix Biol 57-58**:** 1-11

9. Robinson KA, Sun M., Barnum C.E., Weiss S.N., Huegel J., Shetye S.S., Lin L., Saez D., Adams S.M., Iozzo R.V., Soslowsky L.J., Birk D.E. (2017) Decorin and biglycan are necessary for maintaining collagen fibril structure, fiber realignment, and mechanical properties of mature tendons. Matrix Biol 64**:** 81-93

10. Ghadiali RS, Guimond S.E., Turnbull J.E., Pisconti A. (2017) Dynamic changes in heparan sulfate during muscle differentiation and ageing regulate myoblast cell fate and FGF2 signalling. Matrix Biol 59**:** 54-68

11. Nystrom A, Bornert O., Kuhl T. (2017) Cell therapy for basement membrane-linked diseases. Matrix Biol 57-58**:** 124-139

12. Uitto J, Has C., Vahidnezhad H., Youssefian L., Bruckner-Tuderman L. (2017) Molecular pathology of the basement membrane zone in heritable blistering diseases:: The paradigm of epidermolysis bullosa. Matrix Biol 57-58**:** 76-85

13. Foster MH (2017) Basement membranes and autoimmune diseases. Matrix Biol 57-58**:** 149-168

14. Borza CM, Su Y., Tran T.L., Yu L., Steyns N., Temple K.J., Skwark M.J., Meiler J., Lindsley C.W., Hicks B.R., Leitinger B., Zent R., Pozzi A. (2017) Discoidin domain receptor 1 kinase activity is required for regulating collagen IV synthesis. Matrix Biol 57-58**:** 258-271

15. Viquez OM, Yazlovitskaya E.M., Tu T., Mernaugh G., Secades P., McKee K.K., Georges-Labouesse E., De A.A., Quaranta V., Yurchenco P., Gewin L.C., Sonnenberg A., Pozzi A., Zent R. (2017) Integrin α6 maintains the structural integrity of the kidney collecting system. Matrix Biol 57-58**:** 244-257

16. Li S, Qi Y., McKee K., Liu J., Hsu J., Yurchenco P.D. (2017) Integrin and dystroglycan compensate each other to mediate laminin-dependent basement membrane assembly and epiblast polarization. Matrix Biol 57-58**:** 272-284

17. Fuki I, Iozzo R.V., Williams K.J. (2000) Perlecan heparan sulfate proteoglycan. A novel receptor that mediates a distinct pathway for ligand catabolism. J. Biol. Chem. 275**:** 25742-25750

18. Christianson HC, Belting M. (2014) Heparan sulfate proteoglycan as a cell-surface endocytosis receptor. Matrix Biol. 35**:** 51-55

19. Feugaing DDS, Tammi R., Echtermeyer F.G., Stenmark H., Kresse H., Smollich M., Schönherr E., Kiesel L., Götte M. (2007) Endocytosis of the dermatan sulfate proteoglycan decorin utilizes multiple pathways and is modulated by epidermal growth factor receptor signaling. Biochimie 89**:** 637-657

20. Hausser H, Schönherr E., Müller M., Liszio C., Bin Z., Fisher L.W., Kresse H. (1998) Receptor-mediated endocytosis of decorin: involvement of leucine-rich repeat structures. Arch. Biochem. Biophys. 349**:** 363-370

21. Lord MS, Chuang C.Y., Melrose J., Davies M.J., Iozzo R.V., Whitelock J.M. (2014) The role of vascular-derived perlecan in modulating cell adhesion, proliferation and growth factor signaling. Matrix Biol 35**:** 112-122

22. Aspberg A, Binkert C., Ruoslahti E. (1995) The versican C-type lectin domain recognizes the adhesion protein tenascin-R. Proc. Natl. Acad. Sci. USA 92**:** 10590-10594

23. Choi S, Kim Y., Park H., Han I.-O., Chung E., Lee S.-Y., Kim Y.-B., Lee J.W., Oh E.-S., Yi J.Y. (2009) Syndecan-2 overexpression regulates adhesion and migration through cooperation with integrin α2. Biochem. Biophys. Res. Commun. 384**:** 231-235

24. Galvagni F, Nardi F., Spiga O., Trezza A., Tarticchio G., Pellicani R., Andreuzzi E., Caldi E., Toti P., Tosi G.M., Santucci A., Iozzo R.V., Mongiat M., Orlandini M. (2017) Dissecting the CD93-Multimerin 2 interaction involved in cell adhesion and migration of the activated endothelium. Matrix Biol. 64**:** 112-127

25. Jung M, Lord M.S., Cheng B., Lyons J.G., Alkhouri H., Hughes J.M., McCarthy S.J., Iozzo R.V., Whitelock J.M. (2013) Mast cells produce novel shorter forms of perlecan that contain functional endorepellin: A role in angiogenesis and wound healing. J. Biol. Chem. 288**:** 3289-3304

26. Walraven M, Hinz B. (2018) Therapeutic approaches to control tissue repair and fibrosis: Extracellular matrix as a game changer. Matrix Biol, In Press

27. Nugent MA, Nugent H.M., Iozzo R.V., Sanchack K., Edelman E.R. (2000) Perlecan is required to inhibit thrombosis after deep vascular injury and contributes to endothelial cell-mediated inhibition of intimal hyperplasia. Proc. Natl. Acad. Sci. U. S. A. 97**:** 6722-6727

28. Zoeller JJ, McQuillan A., Whitelock J., Ho S.-Y., Iozzo R.V. (2008) A central function for perlecan in skeletal muscle and cardiovascular development. J. Cell Biol. 181**:** 381-394

29. Andreuzzi E, Colladel R., Pellicani R., Tarticchio G., Cannizzaro R., Spessotto P., Bussolati B., Brossa A., De P.P., Canzonieri V., Iozzo R.V., Colombatti A., Mongiat M. (2017) The angiostatic molecule Multimerin 2 is processed by MMP-9 to allow sprouting angiogenesis. Matrix Biol. 64**:** 40-53

30. Wight TN (2018) A role for proteoglycans in vascular disease. Matrix Biol, In Press

31. Patel VN, Pineda D.L., Hoffman M.P. (2017) The function of heparan sulfate during branching morphogenesis. Matrix Biol 57-58**:** 311-323

32. Buraschi S, Neill T., Goyal A., Poluzzi C., Smythies J., Owens R.T., Schaefer L., Torres A., Iozzo R.V. (2013) Decorin causes autophagy in endothelial cells via Peg3. Proc. Natl. Acad. Sci. U. S. A. 110**:** E2582-E2591

33. Poluzzi C, Casulli J., Goyal A., Mercer T.J., Neill T., Iozzo R.V. (2014) Endorepellin evokes autophagy in endothelial cells. J. Biol. Chem. 289**:** 16114-16128

34. Ning L, Xu Z., Furuya N., Nonaka R., Yamada Y., Arikawa-Hirasawa E. (2015) Perlecan inhibits autophagy to maintain muscle homeostasis in mouse soleus muscle. Matrix Biol. 48**:** 26-35

35. Conde-Knape K (2001) Heparan sulfate proteoglycans in experimental models of diabetes: a role for perlecan in diabetes complications. Diabetes Metab. Res. Rev. 17**:** 412-421

36. Gubbiotti MA, Vallet S.D., Ricard-Blum S., Iozzo R.V. (2016) Decorin interacting network: A comprehensive analysis of decorin-binding partners and their versatile functions. Matrix Biol 55**:** 7-21

37. Neill T, Schaefer L., Iozzo R.V. (2012) Decorin, a guardian from the matrix. Am. J. Pathol. 181**:** 380-387

38. Rhodes DR, Yu J., Shanker K., Deshpande N., Varambally R., Ghosh D., Barrette T., Pandey A., Chinnaiyan A.M. (2004) Large-scale meta-analysis of cancer microarray data identifies common transcriptional profiles of neoplastic transformation and progression. Proc. Natl. Acad. Sci. USA 101**:** 9309-9314

39. Chau Y-P, Lin J.-Y., Chen J.H.-C., Tai M.-H. (2003) Endostatin induces autophagic cell death in EAhy926 human endothelial cells. Histol. Histopathol 18**:** 715-726

40. Nguygen TMB, Subramanian I.V., Kelekar A., Ramakrishnan S. (2007) Kringle 5 of human plasminogen, an angiogenesis inhibitor, induces both autophagy and apoptotic death in endothelial cells. Blood 109**:** 4793-4802

41. Gubbiotti MA, Neill T., Iozzo R.V. (2017) A current view of perlecan in physiology and pathology: A mosaic of functions. Matrix Biol 57-58**:** 285-298

42. Gonzalez EM, Reed C.C., Bix G., Fu J., Zhang Y., Gopalakrishnan B., Greenspan D.S., Iozzo R.V. (2005) BMP-1/Tolloid-like metalloproteases process endorepellin, the angiostatic C-terminal fragment of perlecan. J. Biol. Chem. 280**:** 7080-7087

43. Cohen IR, Murdoch A.D., Naso M.F., Marchetti D., Berd D., Iozzo R.V. (1994) Abnormal expression of perlecan proteoglycan in metastatic melanomas. Cancer Res. 54**:** 5771-5774

44. Aviezer D, Iozzo R.V., Noonan D.M., Yayon A. (1997) Suppression of autocrine and paracrine functions of basic fibroblast growth factor by stable expression of perlecan antisense cDNA. Mol. Cell. Biol. 17**:** 1938-1946

45. Cohen IR, Grässel S., Murdoch A.D., Iozzo R.V. (1993) Structural characterization of the complete human perlecan gene and its promoter. Proc. Natl. Acad. Sci. U. S. A. 90**:** 10404-10408

46. Iozzo RV, Pillarisetti J., Sharma B., Murdoch A.D., Danielson K.G., Uitto J., Mauviel A. (1997) Structural and functional characterization of the human perlecan gene promoter. Transcriptional activation by transforming factor-β via a nuclear factor 1-binding element. J. Biol. Chem. 272**:** 5219-5228

47. Iozzo RV, Zoeller J.J., Nyström A. (2009) Basement membrane proteoglycans: Modulators *par excellence* of cancer growth and angiogenesis. Mol. Cells 27**:** 503-513

48. Iozzo RV, Cohen I. (1993) Altered proteoglycan gene expression and the tumor stroma. Experientia 49**:** 447-455

49. Iozzo RV, Cohen I.R., Grässel S., Murdoch A.D. (1994) The biology of perlecan: the multifaceted heparan sulphate proteoglycan of basement membranes and pericellular matrices. Biochem. J. 302**:** 625-639

50. Iozzo RV (2005) Basement membrane proteoglycans: from cellar to ceiling. Nat. Rev. Mol. Cell Biol. 6**:** 646-656

51. San Antonio JD, Zoeller J.J., Habursky K., Turner K., Pimtong W., Burrows M., Choi S., Basra S., Bennett J.S., DeGrado W.F., Iozzo R.V. (2009) A key role for the integrin α2β1 in experimental and developmental angiogenesis. Am. J. Pathol. 175**:** 1338-1347

52. Zoeller JJ, Whitelock J., Iozzo R.V. (2009) Perlecan regulates developmental angiogenesis by modulating the VEGF-VEGFR2 axis. Matrix Biol. 28**:** 284-291

53. Goyal A, Pal N., Concannon M., Paulk M., Doran M., Poluzzi C., Sekiguchi K., Whitelock J.M., Neill T., Iozzo R.V. (2011) Endorepellin, the angiostatic module of perlecan, interacts with both the α2β1 integrin and vascular endothelial growth factor receptor 2 (VEGFR2). J. Biol. Chem. 286**:** 25947-25962

54. Mongiat M, Sweeney S., San Antonio J.D., Fu J., Iozzo R.V. (2003) Endorepellin, a novel inhibitor of angiogenesis derived from the C terminus of perlecan. J. Biol. Chem. 278**:** 4238-4249

55. Bix G, Fu J., Gonzalez E., Macro L., Barker A., Campbell S., Zutter M.M., Santoro S.A., Kim J.K., Höök M., Reed C.C., Iozzo R.V. (2004) Endorepellin causes endothelial cell disassembly of actin cytoskeleton and focal adhesions through the α2β1 integrin. J. Cell Biol. 166**:** 97-109

56. Bix G, Iozzo R.V. (2005) Matrix revolutions: "tails" of basement-membrane components with angiostatic functions. Trends Cell Biol. 15**:** 52-60

57. Bix G, Castello R., Burrows M., Zoeller J.J., Weech M., Iozzo R.A., Cardi C., Thakur M.T., Barker C.A., Camphausen K.C., Iozzo R.V. (2006) Endorepellin in vivo: targeting the tumor vasculature and retarding cancer growth and metabolism. J. Natl. Cancer Inst. 98**:** 1634-1646

58. Douglass S, Goyal A., Iozzo R.V. (2015) The role of perlecan and endorepellin in the control of tumor angiogenesis and endothelial cell autophagy. Connect. Tissue Res. 19**:** 1-11

59. Goyal A, Poluzzi C., Willis A.C., Smythies J., Shellard A., Neill T., Iozzo R.V. (2012) Endorepellin affects angiogenesis by antagonizing diverse VEGFR2- evoked signaling pathways: transcriptional repression of HIF-1α and VEGFA and concurrent inhibition of NFAT1 activation. J. Biol. Chem. 287**:** 43543-43556

60. Willis CD, Poluzzi C., Mongiat M., Iozzo R.V. (2013) Endorepellin laminin-like globular repeat 1/2 domains bind Ig3-5 of vascular endothelial growth factor(VEGF) receptor 2 and block pro-angiogenic signaling by VEGFA in endothelial cells. FEBS J. 280**:** 2271-2294

61. Bix G, Iozzo R.A., Woodall B., Burrows M., McQuillan A., Campbell S., Fields G.B., Iozzo R.V. (2007) Endorepellin, the C-terminal angiostatic module of perlecan, enhances collagen-platelet responses via the α2β1 integrin receptor. Blood 109**:** 3745-3748

62. Woodall BP, Nyström A., Iozzo R.A., Eble J.A., Niland S., Krieg T., Eckes B., Pozzi A., Iozzo R.V. (2008) Integrin α2β1 is the required receptor for endorepellin angiostatic activity. J. Biol. Chem. 283**:** 2335-2343

63. Willis, C. D., Schaefer, L., and Iozzo, R. V. (2012) The biology of perlecan and its bioactive modules. In Karamanos, N. K., editor. *Extracellular Matrix: Pathobiology and Signaling*, Walter de Gruyter GmbH & Co. KG, Berlin

64. Torres A, Gubbiotti M.A., Iozzo R.V. (2017) Decorin-inducible Peg3 Evokes Beclin 1-mediated Autophagy and Thrombospondin 1-mediated Angiostasis. J. Biol Chem. 292**:** 5055-5069

65. Goyal A, Neill T., Owens R.T., Schaefer L., Iozzo R.V. (2014) Decorin activates AMPK, an energy sensor kinase, to induce autophagy in endothelial cells. Matrix Biol. 34**:** 46-54

66. Thoreen CC, Kang S.A., Chang J.W., Liu Q., Zhang J., Gao Y., Reichling L.J., Sim T., Sabatini D.M., Gray N.S. (2009) An ATP-competitive mammalian target of rapamycin inhibitor reveals rapamycin-resistant functions of mTORC1. J. Biol. Chem. 284**:** 8023-8032

67. Gubbiotti MA, Iozzo R.V. (2015) Proteoglycans regulate autophagy via outside-in signaling: An emerging new concept. Matrix Biol. 48**:** 6-13

68. White E (2012) Deconvoluting the context-dependent role for autophagy in cancer. Nat. Rev. Cancer 12**:** 401-410

69. Neill T, Schaefer L., Iozzo R.V. (2015) An oncosuppressive role for decorin. Mol. Cell. Oncol. 2**:** e975645

70. Neill T, Schaefer L., Iozzo R.V. (2016) Decorin as a multivalent therapeutic agent against cancer. Adv. Drug Deliv. Rev. 97**:** 174-185

71. Buraschi S, Neill T., Owens R.T., Iniguez L.A., Purkins G., Vadigepalli R., Evans B., Schaefer L., Peiper S.C., Wang Z., Iozzo R.V. (2012) Decorin protein core affects the global gene expression profile of the tumor microenvironment in a triple-negative orthotopic breast carcinoma xenograft model. PLoS ONE 7**:** e45559

72. Araki K, Wakabayashi H., Shintani K., Morikawa J., Matsumine A., Kusuzaki K., Sudo A., Uchida A. (2009) Decorin suppresses bone metastasis in a breast cancer cell line. Oncology 77**:** 92-99

73. Edwards IJ (2012) Proteoglycans in prostate cancer. Nat. Rev. Urology 9**:** 196-206

74. Karousou E, Misra S., Ghatak S., Dobra K., Gotte M., Vigetti D., Passi A., Karamanos N.K., Skandalis S.S. (2017) Roles and targeting of the HAS/hyaluronan/CD44 molecular system in cancer. Matrix Biol 59**:** 3-22

75. Bissell MJ, Radisky D. (2001) Putting tumors in context. Nat. Rev. Cancer 1**:** 46-54

76. Bissell MJ, Hines W.C. (2011) Why don't we get more cancer? A proposed role of the microenvironment in restraining cancer progression. Nat. Med. 17**:** 320-329

77. Dvorak HF, Weaver V.M., Tlsty T.D., Bergers G. (2011) Tumor Microenvironment and Progression. J. Surg. Oncol. 103**:** 468-474

78. Egeblad M, Rasch M.G., Weaver V.M. (2010) Dynamic interplay between the collagen scaffold and tumor evolution. Current Opinion Cell Biol. 22**:** 697-706

79. Quail DF, Joyce J.A. (2013) Microenvironmental regulation of tumor progression and metastasis. Nat. Med. 19**:** 1423-1437

80. Butler JM, Kobayashi H., Rafii S. (2010) Instructive role of the vascular niche in promoting tumour growth and tissue repair by angiocrine factors. Nat. Rev. Cancer 10**:** 138-146

81. Tanida I, Mimematsu-Ikeguchi N., Ueno T., Kominami E. (2005) Lysosomal turnover, but not a cellular level, of endogenous LC3 is a marker of autophagy. Autophagy 1**:** 84-91

82. Klionsky DJ, Abdelmohsen K., Abe A., Abedin M.J., Abeliovich H., Acevedo A.A., Adachi H., Adams C.M., Adams P.D., Adeli K., Adhihetty P.J., Adler S.G., Agam G., Agarwal R., Aghi M.K., Agnello M., Agostinis P., Aguilar P.V., Aguirre-Ghiso J., Airoldi E.M., Ait-Si-Ali S., Akematsu T., Akporiaye E.T., Al-Rubeai M., Albaiceta G.M., Albanese C., Albani D., Albert

M.L., Aldudo J., Algul H., Alirezaei M., Alloza I., Almasan A., Almonte-Beceril M., Alnemri E.S., Alonso C., Altan-Bonnet N., Altieri D.C., Alvarez S., Alvarez-Erviti L., Alves S., Amadoro G., Amano A., Amantini C., Ambrosio S., Amelio I., Amer A.O., Amessou M., Amon A., An Z., Anania F.A., Andersen S.U., Andley U.P., Andreadi C.K., Andrieu-Abadie N., Anel A., Ann D.K., Anoopkumar-Dukie S., Antonioli M., Aoki H., Apostolova N., Aquila S., Aquilano K., Araki K., Arama E., Aranda A., Araya J., Arcaro A., Arias E., Arimoto H., Ariosa A.R., Armstrong J.L., Arnould T., Arsov I., Asanuma K., Askanas V., Asselin E., Atarashi R., Atherton S.S., Atkin J.D., Attardi L.D., Auberger P., Auburger G., Aurelian L., Autelli R., Avagliano L., Avantaggiati M.L., Avrahami L., Awale S., Azad N., Bachetti T., Backer J.M., Bae D.H., Bae J.S., Bae O.N., Bae S.H., Baehrecke E.H., Baek S.H., Baghdiguian S., Bagniewska-Zadworna A., Bai H., Bai J., Bai X.Y., Bailly Y., Balaji K.N., Balduini W., Ballabio A., Balzan R., Banerjee R., Banhegyi G., Bao H., Barbeau B., Barrachina M.D., Barreiro E., Bartel B., Bartolome A., Bassham D.C., Bassi M.T., Bast R.C., Jr., Basu A., Batista M.T., Batoko H., Battino M., Bauckman K., Baumgarner B.L., Bayer K.U., Beale R., Beaulieu J.F., Beck G.R., Jr., Becker C., Beckham J.D., Bedard P.A., Bednarski P.J., Begley T.J., Behl C., Behrends C., Behrens G.M., Behrns K.E., Bejarano E., Belaid A., Belleudi F., Benard G., Berchem G., Bergamaschi D., Bergami M., Berkhout B., Berliocchi L., Bernard A., Bernard M., Bernassola F., Bertolotti A., Bess A.S., Besteiro S., Bettuzzi S., Bhalla S., Bhattacharyya S., Bhutia S.K., Biagosch C., Bianchi M.W., Biard-Piechaczyk M., Billes V., Bincoletto C., Bingol B., Bird S.W., Bitoun M., Bjedov I., Blackstone C., Blanc L., Blanco G.A., Blomhoff H.K., Boada-Romero E., Bockler S., Boes M., Boesze-Battaglia K., Boise L.H., Bolino A., Boman A., Bonaldo P., Bordi M., Bosch J., Botana L.M., Botti J., Bou G., Bouche M., Bouchecareilh M., Boucher M.J., Boulton M.E., Bouret S.G., Boya P., Boyer-Guittaut M., Bozhkov P.V., Brady N., Braga V.M., Brancolini C., Braus G.H., Bravo-San Pedro J.M., Brennan L.A., Bresnick E.H., Brest P., Bridges D., Bringer M.A., Brini M., Brito G.C., Brodin B., Brookes P.S., Brown E.J., Brown K., Broxmeyer H.E., Bruhat A., Brum P.C., Brumell J.H., Brunetti-Pierri N., Bryson-Richardson R.J., Buch S., Buchan A.M., Budak H., Bulavin D.V., Bultman S.J., Bultynck G., Bumbasirevic V., Burelle Y., Burke R.E., Burmeister M., Butikofer P., Caberlotto L., Cadwell K., Cahova M., Cai D., Cai J., Cai Q., Calatayud S., Camougrand N., Campanella M., Campbell G.R., Campbell M., Campello S., Candau R., Caniggia I., Cantoni L., Cao L., Caplan A.B., Caraglia M., Cardinali C., Cardoso S.M., Carew J.S., Carleton L.A., Carlin C.R., Carloni S., Carlsson S.R., Carmona-Gutierrez D., Carneiro L.A., Carnevali O., Carra S., Carrier A., Carroll B. (2016) Guidelines for the use and interpretation of assays for monitoring autophagy (3rd edition). Autophagy. 12**:** 1-222

83. Saito T, Sadoshima J. (2015) Molecular mechanisms of mitochondrial autophagy/mitophagy in the heart. Circ. Res. 116**:** 1477-1490

84. Vincow ES, Merrihew G., Thomas R.E., Shulman N.J., Beyer R.P., MacCoss M.J., Pallanck L.J. (2013) The PINK1-Parkin pathway promotes both mitophagy and selective respiratory chain turnover in vivo. Proc. Natl. Acad. Sci U. S. A. 110**:** 6400-6405

85. Hirota Y, Yamashita S., Kurihara Y., Jin X., Aihara M., Saigusa T., Kang D., Kanki T. (2015) Mitophagy is primarily due to alternative autophagy and requires the MAPK1 and MAPK14 signaling pathways. Autophagy. 11**:** 332-343

86. Kukat C, Larsson N.G. (2013) mtDNA makes a U-turn for the mitochondrial nucleoid. Trends Cell Biol 23**:** 457-463

87. Kukat C, Wurm C.A., Spahr H., Falkenberg M., Larsson N.G., Jakobs S. (2011) Super-resolution microscopy reveals that mammalian mitochondrial nucleoids have a uniform size and frequently contain a single copy of mtDNA. Proc. Natl. Acad. Sci. U. S. A 108**:** 13534-13539

88. Goyal A, Gubbiotti M.A., Chery D.R., Han L., Iozzo R.V. (2016) Endorepellin-evoked autophagy contributes to angiostasis. J. Biol. Chem. 291**:** 19245-19256

89. Kuhajda FP (2008) AMP-activated protein kinase and human cancer: cancer metabolism revisited. Int. J. Obesity 32**:** S36-S41

90. Kim J, Kundu M., Viollet B., Guan K.-L. (2011) AMPK and mTOR regulate autophagy through direct phopshorylation of Ulk1. Nat. Cell Biol. 13**:** 132-141

91. Cossarizza A, Baccarani-Contri M., Kalashnikova G., Franceschi C. (1993) A new method for the cytofluorimetric analysis of mitochondrial membrane potential using the J-aggregate forming lipophilic cation 5,5',6,6'-tetrachloro-1,1',3,3'-tetraethylbenzimidazolcarbocyanine iodide (JC-1). Biochem. Biophys. Res. Comm. 197**:** 40-45

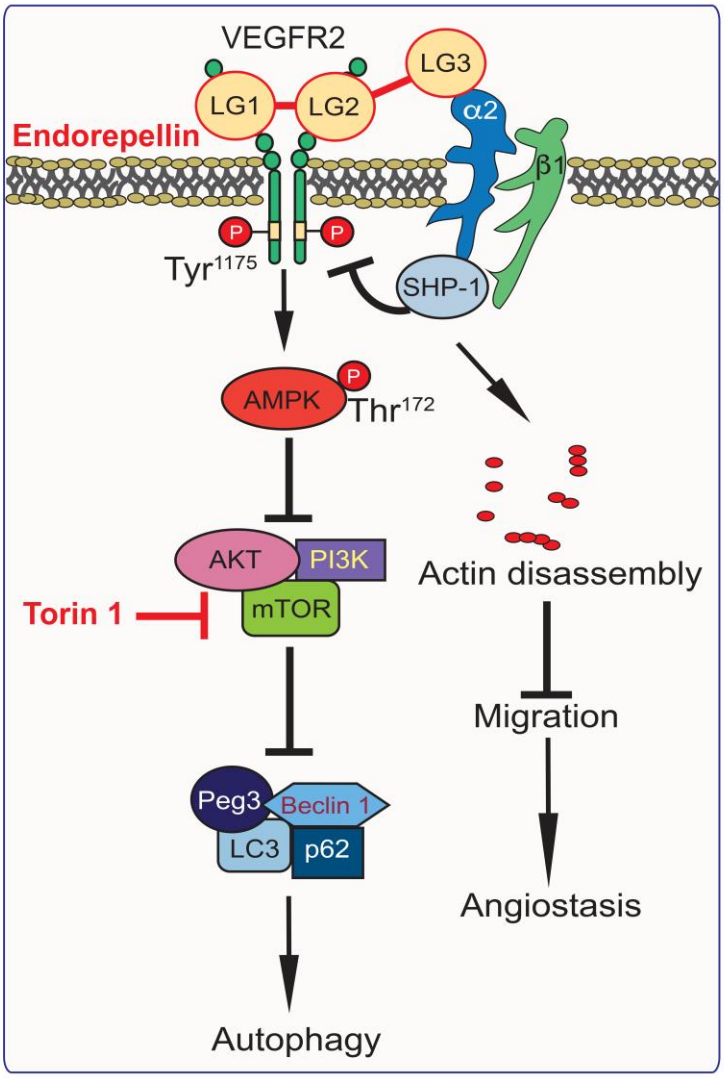

Fig. 1. Working model depicting the mechanism of action of endorepellin and Torin 1 (both red). Endorepellin is an angiostatic and pro-autophagic factor. Torin 1 is a pro-autophagic factor.

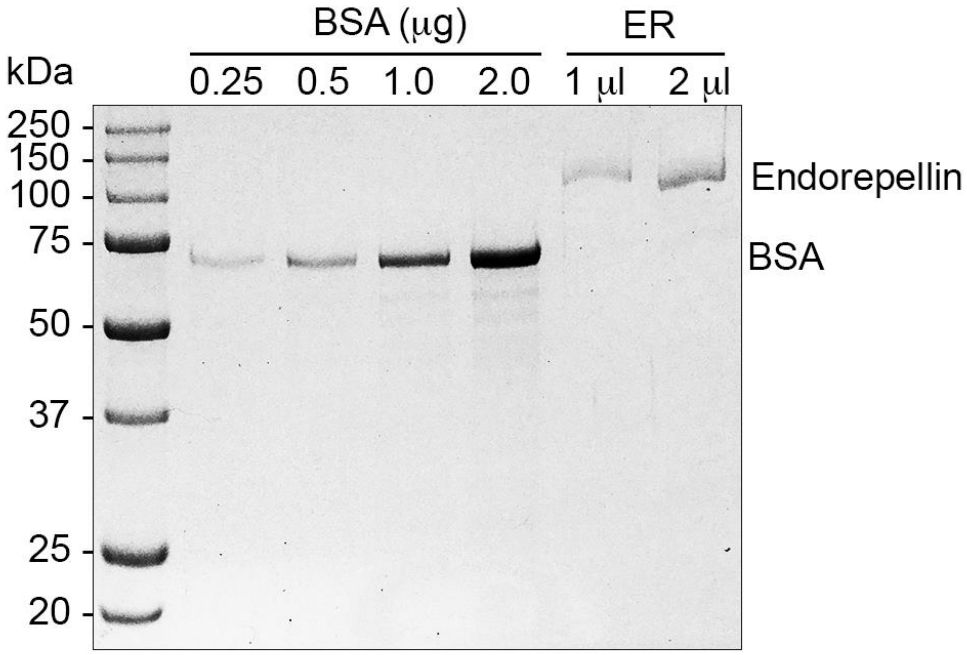

Fig. 2. Example of purified recombinant endorepellin run alongside a BSA concentration curve. The 10% acrylamide gel was run at 18 mA, stained with Coomassie Brilliant Blue dye for 30 min, and destained for 36 h. The calculated concentration of this endorepellin purification is 0.25 mg/ml.

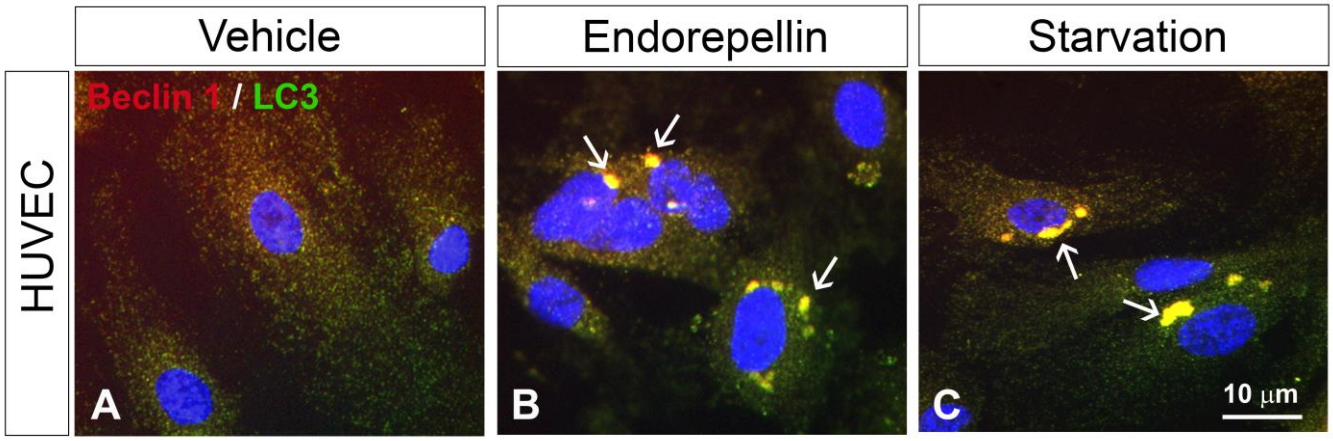

Fig. 3. Visualizing matrix-induced autophagosomes *in vitro.* Representative immunofluorescence images of HUVEC treated with vehicle (A), endorepellin (200 nM, 4 h) (B), and serum-starved (HBSS, 4 h) (C). Cells were dually stained with antibodies against Beclin 1 (red) and LC3 (green), with prominent autophagosomes showing colocalization (yellow, arrows). Scale bar = 10 μm.

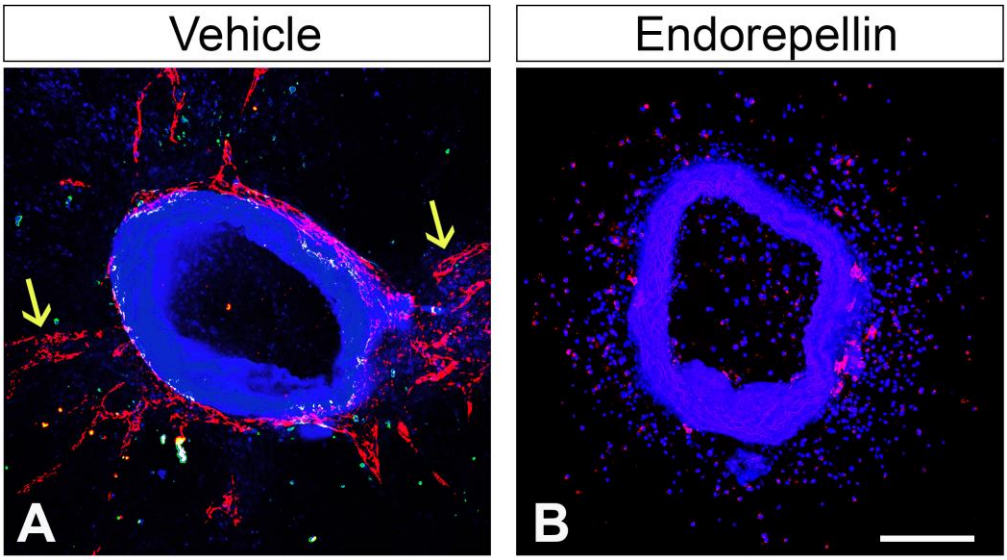

Fig. 4. Confocal microscopy depicting the difference in microvessel growth between vehicle (PBS) and recombinant endorepellin-treated rings. (A) Dense, long sprouts (yellow arrows) emanating from control aortic rings treated with Vehicle (PBS). Rings were stained with CD31 (red). (B). Collapsed microvessels in aortic rings treated with endorepellin (200 nM). Rings were stained with CD31 (red). Scale bar = 300 μm.

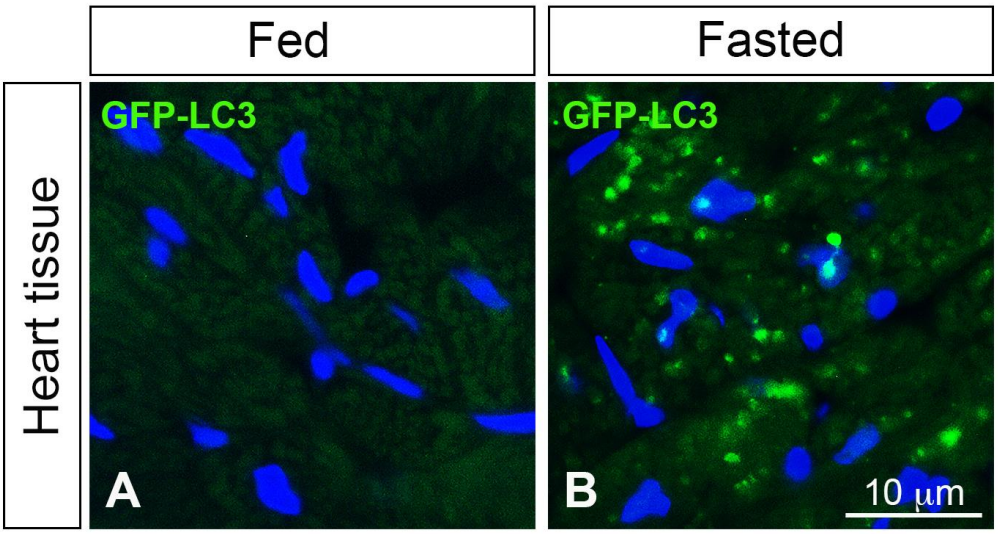

Fig. 5. LC3 puncta formation in heart tissue of fasted GFP-LC3 transgenic mice ablated in GFP-LC3;*Dcn-/-* mice. (A-D) Representative immunohistochemistry images of heart sections from GFP-LC3 mice that were fed (A) or fasted for 25 h (B), showing increased LC3 puncta in fasted hearts. Heart sections from GFP-LC3;*Dcn-/-* that were fed (C) or fasted for 25 h (D) did not show this increase in puncta formation.

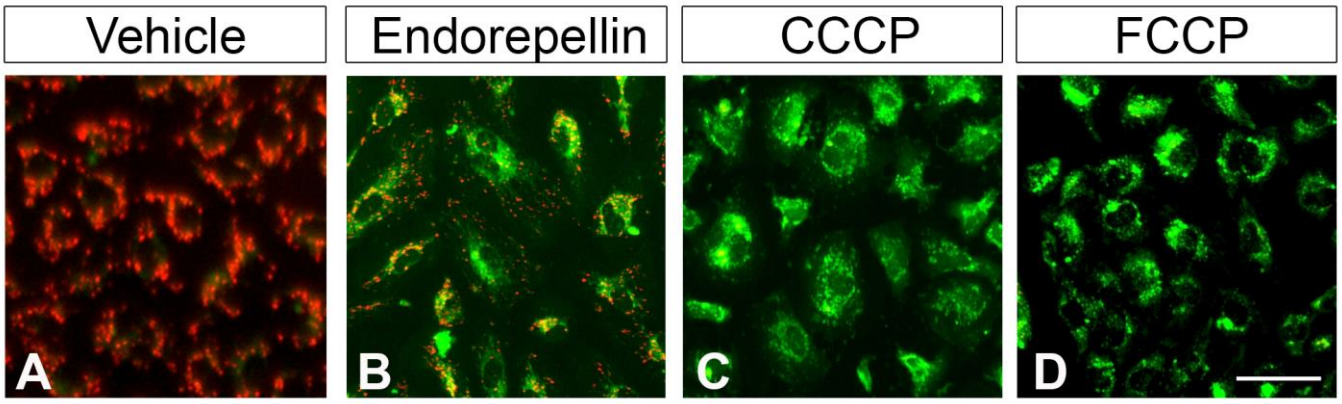

Fig. 6. Visualizing mitochondrial depolarization via JC-1 staining. (A-D) Representative fluorescence micrographs depicting live cell imaging of HUVEC after incubation with vehicle (A), endorepellin (6 h) (B), CCCP (1 h, 30 μM) (C), or FCCP (10 min, 500 nM) (D). HUVEC were cultured in nutrient-rich media and incubated with JC-1 (20 min, 7.5 μM) to assess mitochondrial membrane potential. Scale bar ~50 μm.

Table 1
Antibodies for Western Blot Analysis

Primary antibody	IHC Dilution	Source organism	Company	Marker
Anti-LC3B	1:1000	Rabbit	Sigma	Autophagosome
Anti-p62/SQSTM1	1:1000	Rabbit	Abcam	Autophagosome
Anti-ATG9A	1:1000	Rabbit	Abcam	Trans-Golgi Network & Endosome/Autophagosome
Anti-GAPDH	1:10000	Rabbit	Cell Signaling	Loading control
Anti-PINK1	1:1000	Rabbit	Cell Signaling	Outer mitochondrial membrane
Anti-ANT	1:1000	Rabbit	Cell Signaling	Outer mitochondrial membrane
Anti-VDAC1	1:1000	Rabbit	Cell Signaling	Outer mitochondrial membrane
Anti-Hsp60	1:1000	Rabbit	Cell Signaling	Mitochondrial matrix
Anti-Mitofusin 2	1:1000	Mouse	Abcam	Outer mitochondrial membrane & Endoplasmic Reticulum
Total OxPhos Human Antibody Cocktail	1:1000	Mouse	Abcam	Mitochondrial Matrix & Inner mitochondrial membrane

Secondary antibody	IHC Dilution	Source organism	Company
Alexa Fluor 488 anti-rabbit IgG	1:400	Goat	Thermo Fisher
Alexa Fluor 594 anti-rabbit IgG	1:400	Donkey	Thermo Fisher
Alexa Fluor 594 anti-mouse IgG	1:400	Rabbit	Thermo Fisher

Table 2
Antibodies for Tissue Immunohistochemistry

Primary antibody	IHC Dilution	Source organism	Company	Marker
Anti-CD31	1:50	Rabbit	Abcam	Endothelial vessels
Anti-LYVE1	1:200	Rabbit	Abcam	Lymphatics
HA binding protein, biotinylated	5 μg/ml	Bovine nasal cartilage	Calbiochem	Hyaluronan
Isolectin GS-IB4 AF594 conjugate	1:300	*Griffonia simplicifolia*	Thermo Fisher	Endothelial vessels
Anti-His_6	1:200	Mouse	BD Pharmingen	His_6-tagged protein
Anti-LC3B	1:200	Rabbit	Sigma	Autophagosome

Secondary antibody	IHC Dilution	Source organism	Company
Alexa Fluor 594 anti-rabbit IgG	1:400	Goat	Thermo Fisher
Streptavidin Alexa Fluor 594	1:400	—	Thermo Fisher
Alexa Fluor 594 anti-mouse IgG	1:400	Rabbit	Thermo Fisher